

Investigation of hollow cylindrical metal terahertz waveguides suitable for cryogenic environments

R. WALLIS,^{1,*} R. DEGL'INNOCENTI,¹ D. S. JESSOP,¹ O. MITROFANOV,² C. M. BLEDT,³ J. E. MELZER,³ J. A. HARRINGTON,³ H. E. BEERE,¹ AND D. A. RITCHIE¹

¹*Cavendish Laboratory, University of Cambridge, JJ Thomson Avenue, Cambridge, CB3 0HE, UK*

²*Department of Electronic and Electrical Engineering, University College London, Torrington Place, London, WC1E 7JE, UK*

³*School of Engineering, Rutgers University, 607 Taylor Road, Piscataway, New Jersey 08854, USA*

*rw497@cam.ac.uk

Abstract: The field of terahertz (THz) waveguides continues to grow rapidly, with many being tailored to suit the specific demands of a particular final application. Here, we explore waveguides capable of enabling efficient and accurate power delivery within cryogenic environments (< 4 K). The performance of extruded hollow cylindrical metal waveguides made of un-annealed and annealed copper, as well as stainless steel, have been investigated for bore diameters between 1.75 - 4.6 mm, and at frequencies of 2.0, 2.85 and 3.4 THz, provided by a suitable selection of THz quantum cascade lasers. The annealed copper resulted in the lowest transmission losses, < 3 dB/m for a 4.6 mm diameter waveguide, along with 90° bending losses as low as ~2 dB for a bend radius of 15.9 mm. The observed trends in losses were subsequently analyzed and related to measured inner surface roughness parameters. These results provide a foundation for the development of a wide array of demanding low-temperature THz applications, and enabling the study of fundamental physics.

Published by The Optical Society under the terms of the [Creative Commons Attribution 4.0 License](https://creativecommons.org/licenses/by/4.0/). Further distribution of this work must maintain attribution to the author(s) and the published article's title, journal citation, and DOI.

OCIS codes: (140.5965) Semiconductor lasers, quantum cascade; (230.7370) Waveguides; (140.3300) Laser beam shaping.

References and links

1. O. Mitrofanov, R. James, F. A. Fernandez, T. K. Mavrogordatos, and J. A. Harrington, "Reducing transmission losses in hollow THz waveguides," *IEEE Trans. Terahertz Sci. Technol.* **1**(1), 124–132 (2011).
2. M. M. Awad and R. A. Cheville, "Transmission terahertz waveguide-based imaging below the diffraction limit," *Appl. Phys. Lett.* **86**(22), 221107 (2005).
3. H. Zhan, R. Mendis, and D. M. Mittleman, "Superfocusing terahertz waves below $\lambda/250$ using plasmonic parallel-plate waveguides," *Opt. Express* **18**(9), 9643–9650 (2010).
4. R. Wallis, R. Degl'Innocenti, D. S. Jessop, Y. Ren, A. Klimont, Y. D. Shah, O. Mitrofanov, C. M. Bledt, J. E. Melzer, J. A. Harrington, H. E. Beere, and D. A. Ritchie, "Efficient coupling of double-metal terahertz quantum cascade lasers to flexible dielectric-lined hollow metallic waveguides," *Opt. Express* **23**(20), 26276–26287 (2015).
5. M. Tonouchi, "Cutting-edge terahertz technology," *Nat. Photonics* **1**(2), 97–105 (2007).
6. A. Cosentino, "Terahertz and cultural heritage science: examination of art and archaeology," *Technologies* **4**(1), 6–19 (2016).
7. C. J. Strachan, P. F. Taday, D. A. Newnham, K. C. Gordon, J. A. Zeitler, M. Pepper, and T. Rades, "Using terahertz pulsed spectroscopy to quantify pharmaceutical polymorphism and crystallinity," *J. Pharm. Sci.* **94**(4), 837–846 (2005).
8. T. Hidaka, H. Minamide, H. Ito, S.-I. Maeta, and T. Akiyama, "Ferroelectric PVDF cladding terahertz waveguide," *Proc. SPIE* **5135**, 70–77 (2003).
9. M. Nagel, A. Marchewka, and H. Kurz, "Low-index discontinuity terahertz waveguides," *Opt. Express* **14**(21), 9944–9954 (2006).
10. M. Goto, A. Quema, H. Takahashi, S. Ono, and N. Sarukura, "Teflon photonic crystal fiber as terahertz waveguide," *Jpn. J. Appl. Phys.* **43**(28), 317–319 (2004).

11. K. Wang and D. M. Mittleman, "Metal wires for terahertz wave guiding," *Nature* **432**(7015), 376–379 (2004).
12. D. R. Grischkowsky, "Optoelectronic characterization of transmission lines and waveguides by terahertz time-domain spectroscopy," *IEEE J. Sel. Top. Quantum Electron.* **6**(6), 1122–1135 (2000).
13. R. W. McGowan, G. Gallot, and D. Grischkowsky, "Propagation of ultrawideband short pulses of terahertz radiation through submillimeter-diameter circular waveguides," *Opt. Lett.* **24**(20), 1431–1433 (1999).
14. P. Doradla and R. H. Giles, "Dual-frequency characterization of bending losses in hollow flexible terahertz waveguides," *Proc. SPIE* **8985**, 898518 (2014).
15. O. Mitrofanov and J. A. Harrington, "Dielectric-lined cylindrical metallic THz waveguides: mode structure and dispersion," *Opt. Express* **18**(3), 1898–1903 (2010).
16. P. Doradla, C. S. Joseph, J. Kumar, and R. H. Giles, "Characterization of bending loss in hollow flexible terahertz waveguides," *Opt. Express* **20**(17), 19176–19184 (2012).
17. G. Gallot, S. P. Jamison, R. W. McGowan, and D. Grischkowsky, "Terahertz waveguides," *J. Opt. Soc. Am. B* **17**(5), 851–863 (2000).
18. J. Harrington, R. George, P. Pedersen, and E. Mueller, "Hollow polycarbonate waveguides with inner Cu coatings for delivery of terahertz radiation," *Opt. Express* **12**(21), 5263–5268 (2004).
19. H. D. Young and R. A. Freedman, *University Physics* (Addison Wesley, 1996).
20. J. R. Davis, *Copper and Copper Alloys* (ASM International, 2001).
21. R. Köhler, A. Tredicucci, F. Beltram, H. E. Beere, E. H. Linfield, A. G. Davies, D. A. Ritchie, R. C. Iotti, and F. Rossi, "Terahertz semiconductor-heterostructure laser," *Nature* **417**(6885), 156–159 (2002).
22. L. Li, L. Chen, J. Zhu, J. Freeman, P. Dean, A. Valavanis, A. G. Davies, and E. H. Linfield, "Terahertz quantum cascade lasers with >1 W output powers," *Electron. Lett.* **50**(4), 309–311 (2014).
23. J. R. Freeman, A. Brewer, J. Madéo, P. Cavalie, S. S. Dhillon, J. Tignon, H. E. Beere, and D. A. Ritchie, "Broad gain in a bound-to-continuum quantum cascade laser with heterogeneous active region," *Appl. Phys. Lett.* **99**(24), 241108 (2011).
24. M. Navarro-Cía, M. S. Vitiello, C. M. Bledt, J. E. Melzer, J. A. Harrington, and O. Mitrofanov, "Terahertz wave transmission in flexible polystyrene-lined hollow metallic waveguides for the 2.5-5 THz band," *Opt. Express* **21**(20), 23748–23755 (2013).
25. S. Barbieri, J. Alton, H. E. Beere, J. Fowler, E. H. Linfield, and D. A. Ritchie, "2.9 THz quantum cascade lasers operating up to 70 K in continuous wave," *Appl. Phys. Lett.* **85**(10), 1674 (2004).
26. M. I. Amanti, G. Scalari, R. Terazzi, M. Fischer, M. Beck, J. Faist, A. Rudra, P. Gallo, and E. Kapon, "Bound-to-continuum terahertz quantum cascade laser with a single-quantum-well phonon extraction/injection stage," *New J. Phys.* **11**(12), 125022 (2009).
27. R. Degl'Innocenti, Y. D. Shah, D. S. Jessop, Y. Ren, O. Mitrofanov, H. E. Beere, and D. A. Ritchie, "Hollow metallic waveguides integrated with terahertz quantum cascade lasers," *Opt. Express* **22**(20), 24439–24449 (2014).
28. J. A. Harrington, *Infrared Fibre Optics and Their Applications* (SPIE, 2004).
29. F. P. Payne and J. P. R. Lacey, "A theoretical analysis of scattering loss from planar optical waveguides," *Opt. Quantum Electron.* **26**(10), 977–986 (1994).
30. Y. Matsuura, A. Hongo, M. Saito, and M. Miyagi, "Loss characteristics of circular hollow waveguides for incoherent infrared light," *J. Opt. Soc. Am. A* **6**(3), 423–427 (1989).
31. C. D. Rabii, D. J. Gibson, and J. A. Harrington, "Processing and characterization of silver films used to fabricate hollow glass waveguides," *Appl. Opt.* **38**(21), 4486–4493 (1999).
32. K. K. Lee, D. R. Lim, H.-C. Luan, A. Agarwal, J. Foresi, and L. C. Kimerling, "Effect of size and roughness on light transmission in a Si/SiO₂ waveguide: Experiments and model," *Appl. Phys. Lett.* **77**(11), 1617 (2000).

1. Introduction

In recent years the field of terahertz (THz) waveguides has made significant progress, both in improving fundamental performance characteristics, such as transmission losses, dispersion and fabrication techniques [1], as well as increasing integration into THz applications previously dominated by free space optics [2,3]. This integration provides multiple benefits, particularly the ability to deliver purgeable, targeted power delivery, which is readily alignable over longer distances (>100 mm) [4]. As the breadth of THz applications continues to increase, including such diverse fields as biomedicine, spectroscopy and security [5], to cultural heritage [6] and pharmaceutical quality control [7], the research into THz waveguides is constantly evolving to meet the specific requirements demanded. As such, there exists a plethora of waveguide designs, encompassing many different geometries and materials, including hollow [8] and solid [9] core dielectric designs, photonic crystal [10], wire [11], coplanar [12], hollow core metallic [13,14], and dielectric lined metallic [15,16], each with their own set of strengths and weaknesses. However, to date, there has been relatively little focus on THz waveguides suitable for delivery in cryogenic environments (< 4 K), within

which there exists the potential for extensive study of samples operating with transitions on the THz scale ($7 - 15 \text{ meV} \approx 1.7 - 3.6 \text{ THz}$).

In this work, we choose to focus attention on developing waveguides suitable for operating effectively in such environments, where delivery of THz radiation has been traditionally challenging. This is due to the fact that for cryogenic operation below 4 K, THz delivery is hindered by multiple cryogenic vacuum chambers, each requiring an absorbing optical window. Thus, a fiber delivery system along the central cryostat axis presents itself as a promising solution. In these environments, the transmission loss becomes especially important due to the large physical distance between source and sample in cryogenic systems. Consequently, a key requirement becomes the ability to fabricate waveguides reliably over long distances ($> 1000 \text{ mm}$). Additionally, for effective sample illumination, a reproducible, Gaussian-like beam is required, and due to the extreme temperature variations involved in thermal cycling, the resulting expansion and contraction of components makes mechanical stability a central requirement for any potential waveguide design. The design which addresses all of these concerns is the cylindrical hollow metallic waveguide (HMWG), the study of which has previously been fairly limited. In 1999, sub-picosecond pulses were first coupled into circular HMWGs [13], and in 2000, Gallot et al. [17] studied circular stainless steel waveguides, with hypodermic needles being chosen for uniformity of the inner wall, which showed a transmission loss of 0.7 cm^{-1} or $\sim 300 \text{ dB/m}$ for a $280 \text{ }\mu\text{m}$ diameter, measured at 1 THz. Designs to produce HMWGs that were also flexible soon followed, which was achieved by coating a dielectric tube with an inner metallic layer [18]. In these designs, the dielectric cladding allows for flexibility, whilst the inner metallic layer provides the optical confinement. However, the use of such dielectric materials renders them susceptible to a lack of mechanical stability at cryogenic temperatures, such as a loss of adhesion between coating layers, and additionally, such designs often possess complex liquid phase fabrication procedures.

Here, we focus on exploring the properties of extruded hollow annealed and un-annealed copper and stainless steel waveguides, with bore diameters between 1.75 and 4.6 mm, and investigate their performance in terms of transmission losses, bending losses, and mode profiles at three separate frequencies. This represents a crucial building block in achieving efficient THz delivery from a room temperature environment into a cryostat. This investigation is achieved via the use of THz QCLs coupled into a hollow dielectric lined metallic waveguide, which is used as a launch structure to clean and normalize the input beam [4] before coupling into the test waveguides. The best waveguides exhibit transmission losses $< 3 \text{ dB/m}$ measured at 2 THz, as well as bending losses of $\sim 2 \text{ dB}$ at 90° for a bend radius of 15.9 mm. Observed variations in losses between metal types and diameters are also explored in terms of surface roughness parameters.

2. Experimental Setup

HMWGs of three different metal types were chosen for investigation – un-annealed copper (UnCu), annealed copper (AnCu) and stainless steel (SS). Copper is an excellent material for THz applications due to its high electrical conductivity, and resulting low skin depth, which minimizes optical penetration and thus ohmic losses. It also has advantages in terms of being both readily malleable, and easily available in a variety of dimensions. Stainless steel was also chosen due to its lower thermal conductivity as compared to copper ($\kappa_{\text{steel}} \approx 50 \text{ W/mK}$ compared to $\kappa_{\text{Cu}} \approx 385 \text{ W/mK}$) [19], which becomes a major consideration in most cryogenic applications. All the waveguides were commercial extruded cylinders, with three different inner diameters - 1.75, 2.5, and 4.6 mm, and wall thicknesses of 0.71, 1.13, and 0.87 mm, respectively. These were chosen to be a practical diameter for typical cryogenic applications, as well as to balance the trade-off that exists when working with THz waveguides between desirable single mode transmission, but at the cost of increasing losses as the diameter is reduced [18]. The primary focus of this work was on UnCu and AnCu waveguides of the

smaller 1.75 mm diameter, for the investigation of single mode transmission, and the larger 4.6 mm diameter, which were expected to possess lower losses. Additionally, the 2.5 mm diameter was included as an intermediate dimension to better understand the transition between the smaller and larger diameters, and to provide additional data to facilitate subsequent analysis. A set of three HMWGs of a particular material and diameter were cut into lengths between 50 and 150 mm, with the ends carefully deburred to maintain the symmetry of the inner wall and minimize irregularities that could have a detrimental effect on optical transmission. The cleaning process consisted of separate 30 second submersions in water, acetone, and isopropyl alcohol, each with ultrasonic agitation. This was followed by a 30 second submersion in a 1:5 HCl:H₂O solution, then a 10 second submersion in a 1:5 HNO₃:H₂O solution, both of which with the aim of removing any surface oxides, as well as residual annealing scale and tarnish [20].

As a radiation source to investigate the waveguide properties, the THz quantum cascade laser (QCL) [21] was chosen due to its many favorable properties, such as the potential for high output powers [22], compactness, and a frequency of emission which is selectable by appropriate design of the active region [23]. Furthermore, in order to deliver the radiation from the QCL to the waveguide under test, and also to clean and normalize the input beam, a 330 mm long, 1 mm diameter flexible polystyrene-lined hollow metallic waveguide (PS-MWG) [24] was used, external to the QCL housing cryostat, at a distance of ~2 mm from the radiation source, as has been previously demonstrated [4]. This type of waveguide, although too mechanically unstable to be appropriate as a cryogenic waveguide candidate itself, has the advantages of relatively low loss (~5 dB/m), and supports a Gaussian-like HE₁₁ mode with a divergence angle of 14°, making it very suitable for launching into the test waveguides efficiently. A length of 330 mm ensured an optimal balance between allowing transmission over a long enough distance for the QCL mode to be cleaned, whilst retaining sufficient power for characterization measurements on the HMWGs.

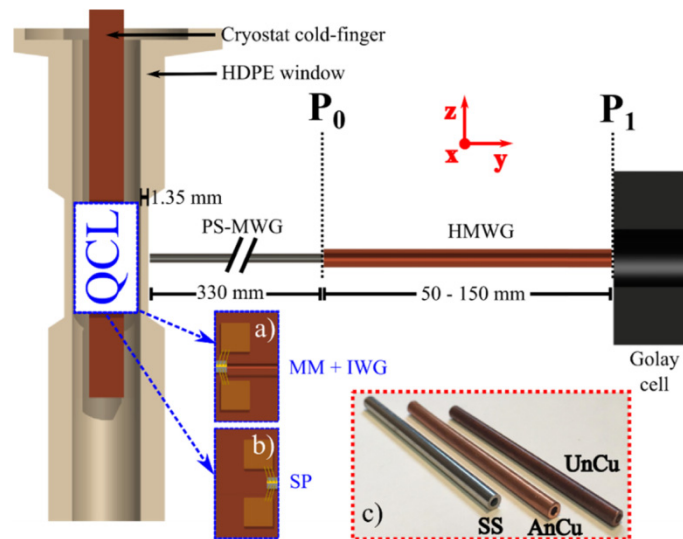


Fig. 1. Schematic of the setup used to characterize the HMWGs. A QCL was placed within the cryostat, and coupled into the external PS-MWG through a cylindrical HDPE window of 1.35 mm wall thickness. For the case of single-plasmon waveguided QCL designs, radiation was directly coupled into the PS-MWG, and for metal-metal waveguided devices, the beam was initially shaped using a copper waveguide monolithically integrated into the mounting block (IWG), prior to out-coupling from the cryostat, in order to increase coupling efficiency [4]. Initial and final powers were measured from the end of the PS-MWG (P_0) and from the end of the HMWG (P_1) respectively using a Golay cell detector. Inset c) – Photograph showing the 1.75 mm diameter SS, AnCu and UnCu waveguides.

The full set up for investigating the HMWGs is shown in Fig. 1. The QCL used as a radiation source was placed on the cold-finger of a continuous-flow He cryostat, with a cylindrical high density polyethylene (HDPE) window of inner diameter 12 mm and 1.35 mm wall thickness. The QCLs were operated in pulsed mode with frequencies between 10 and 100 kHz, and 2% duty cycle. Radiation was coupled into the external PS-MWG, followed by the HMWG under test, which was placed with the input end in the same plane as the output end of the PS-MWG, and with axes aligned. Initial and final intensities were recorded from the output end of the PS-MWG (P_0) and HMWG (P_1) respectively, via the use of a Golay cell detector and lock-in detection at 24 Hz.

QCLs with three different active regions were selected in order to investigate the HMWG performance over three frequency ranges [see Fig. 2(a)]. The first was a bound-to-continuum design [25] operating with primarily single mode emission at 2.0 THz (red), fabricated in a single-plasmon (SP) waveguide architecture. The second was a bound-to-continuum design operating at 2.85 THz (green), and the third was a hybrid bound-to-continuum with LO phonon extraction design [26] operating with multimode emission between $\sim 3.2 - 3.4$ THz (blue), both with metal-metal (MM) waveguide. The SP device was directly coupled into the external waveguide [Fig. 1(a)], and the MM devices were first coupled into a hollow cylindrical copper waveguide monolithically integrated into the laser mounting block (IWG) [4,27], [Fig. 1(b)], in order to shape the highly divergent beam profiles characteristic of MM devices, and increase the coupling efficiency into the external PS-MWG. The far field profile from the PS-MWG was examined for each device prior to coupling into any test waveguides, and was recorded using a Golay cell detector with 1 mm aperture, scanned in the plane perpendicular to the waveguide axis at a distance of 4.5 mm. A representative profile is shown in Fig. 2(b) for the 2.0 THz QCL, which exhibited the fundamental Gaussian-like HE_{11} mode of the structure, and provided an excellent launch beam with which to efficiently couple into the HMWGs. Similar profiles were also recorded for the 2.85 and 3.2 THz QCLs (not shown). Three lengths of each waveguide were measured for a fixed frequency, bore diameter, and material type, with lengths of 50, 100, and 150 mm forming a set, in order to allow the coupling losses to be distinguished from the transmission losses for each. These lengths were chosen for ease of fabrication and cleaning, and also to allow accurate power measurements within the sensitivity range of the Golay cell detector used.

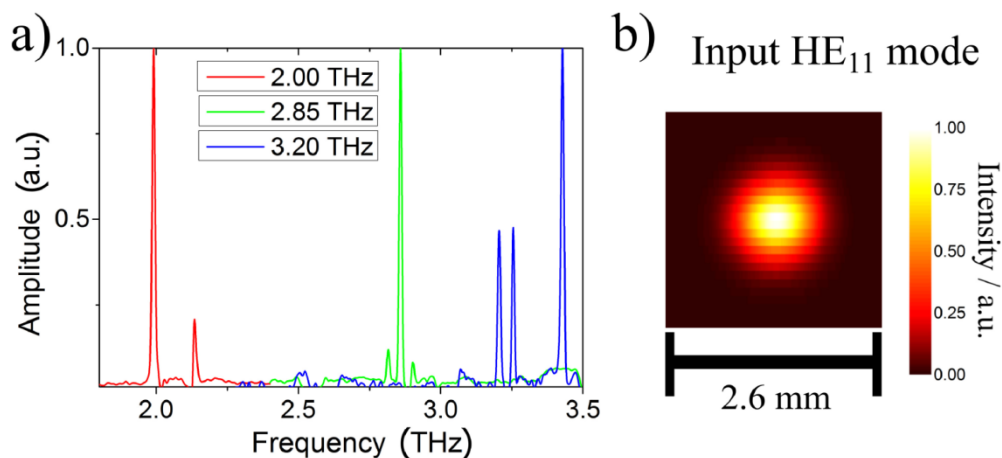


Fig. 2. a) Frequency spectra for the three QCL devices used to characterize the HMWGs, showing quasi-single mode operation at 2.0 THz (red), and 2.85 THz (green), and multimode emission for the hybrid active region device between 3.2 and 3.4 THz (blue). b) Representative far field profile from the end of the PS-MWG using the 2.0 THz device, showing the Gaussian-like HE_{11} mode used as a launch beam. The same mode was observed for all three QCLs used.

3. Results

For a given set of waveguides of particular material and diameter, the initial and final powers were recorded for each of the three lengths, allowing the loss to be determined as a function of length. A linear fit then provided both the coupling loss from the intercept, and the transmission loss from the gradient. An exemplary plot for the 1.75 mm AnCu waveguide at 3.2 THz is shown in Fig. 3.

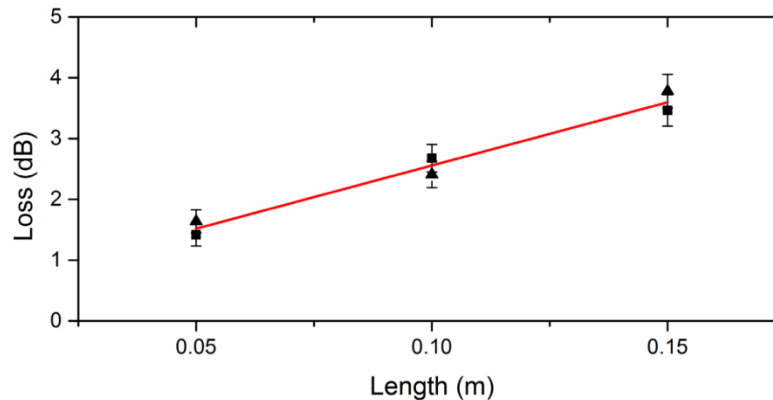


Fig. 3. Exemplary plot of loss as a function of waveguide length for the case of the 1.75 mm diameter AnCu waveguide, measured at 3.2 THz. A linear fit (red) provides the coupling loss from the intercept, and the transmission loss from the gradient. The squares and triangles represent data from two separate measuring runs, showing the reproducibility of the measurements.

The resulting transmission losses for all the sets of waveguides tested are shown in Fig. 4. The left hand panel shows the losses for 1.75 mm bore diameter waveguides, the middle panel 2.5 mm diameters, and the right hand panel the 4.6 mm diameter waveguides. The three frequencies tested for each diameter and material are shown in solid red (2.0 THz), up-hatched green (2.85 THz), and down-hatched blue (3.2 THz). With atmospheric water absorption being so prevalent across the entire THz frequency range, measurements were taken both with the waveguides purged with nitrogen gas (solid bars) and un-purged (faded bars), with a relative humidity of 38%, to control for the influence of atmospheric absorption on measured losses.

As can be seen, the measured losses vary by a considerable amount, depending on the choice of material, frequency and diameter, from up to ~ 30 dB/m for a 1.75 mm UnCu waveguide, down to < 3 dB/m for the 4.6 mm AnCu waveguide set, a value comparable to previously reported, but more structurally complex designs [18]. In addition, this value is also sufficiently low to allow such a waveguide to be effectively implemented into fiber-coupled cryogenic delivery systems with path lengths in excess of 1 meter, whilst retaining sufficient signal. From Fig. 4 taken as a whole, there appears to be three primary observations to be made. The first is the trend for lower transmission loss as the bore diameter increases, for a given frequency and material. This is generally attributed to a larger proportion of the optical mode propagating within the hollow core of the waveguide for larger bore diameters [15,18]. The second is that for a given bore diameter and material, a consistent increase in losses is observed as measurements are performed from lower to higher frequencies (solid red to down-hatched blue). Such a pronounced effect was unexpected, especially after correcting for atmospheric absorption. The third observation is that for the 1.75 and 4.6 mm diameter waveguides measured, the AnCu waveguide appears to support a considerably lower loss than the equivalent un-annealed version. For example, for a 1.75 mm diameter at 2.0 THz, the loss is reduced by ~ 10 dB/m by moving to the AnCu waveguide. Potential mechanisms for these trends are discussed in the next section.

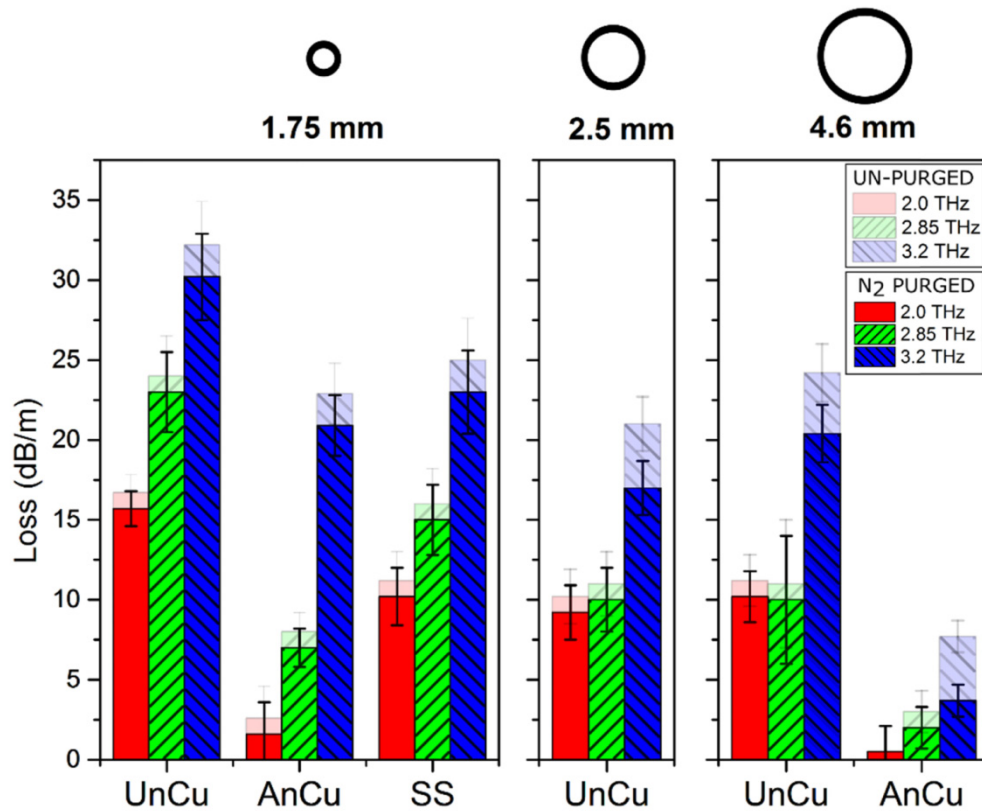


Fig. 4. Transmission losses recorded with waveguides of varying material, bore diameter, and at varying frequencies. Bore diameters ranged from 1.75 mm (left panel), 2.5 mm (middle panel), and 4.6 mm (right panel). The three frequencies tested are shown as solid red (2.0 THz), up-hatched green (2.85 THz) and down-hatched blue (3.2 THz). Faded bars show measurements taken in standard atmosphere with a relative humidity of 38%, and solid bars show measurements taken whilst purging with nitrogen gas.

Another important characteristic of any waveguide is the mode structures supported. These were analyzed by recording the beam profile from the end of each HMWG using a Golay cell detector with 1 mm aperture at a distance of 4.5 mm, which was mounted on a motorized x-y stage and scanned in the plane perpendicular to the beam. The profiles were acquired with the PS-MWG axis centrally aligned and parallel to the axis of the HMWG in each case. Profiles for each combination of material and diameter are shown in Fig. 5(a), along with the theoretical lower order TE_{01} , TE_{11} , TM_{01} , and TM_{11} modes that can be supported by such cylindrical HMWGs in Fig. 5(b), as calculated by finite element analysis (FEA) simulations. It should be noted that theoretically, the doughnut shaped TE_{01} mode has the lowest loss in such structures, but due to its circularly polarized nature, coupled with the fact that the exciting QCL is linearly polarized, it was not expected to be the primary mode excited. The results in Fig. 5(a) clearly show that for the 1.75 mm diameter waveguides, transmission is primarily single mode, with the TE_{11} mode being observed. As the bore diameter is increased, the introduction of higher order modes is observed, with the appearance of annular, multi-lobed distributions suggestive of TM_{11} mode content, especially in the case of the 2.5 mm diameter. Despite this marginal degradation in the beam quality for the larger diameters, it is interesting to note that in the case of the 4.6 mm diameter AnCu waveguide, the single-lobed nature of the beam is still maintained despite some lateral extension in one axis, which is key from an applications standpoint, although the presence of higher order modes cannot be ruled out. Another point of note in the case of the 1.75 mm waveguides was

the lower tolerance to misalignment between waveguides. This was observed by measuring the degree of lateral misalignment tolerated until the recorded power dropped to half of the original, as measured from the waveguide exit, which was found to be 750, 1000 and 1680 μm in the case of 1.75, 2.5 and 4.6 mm diameters respectively.

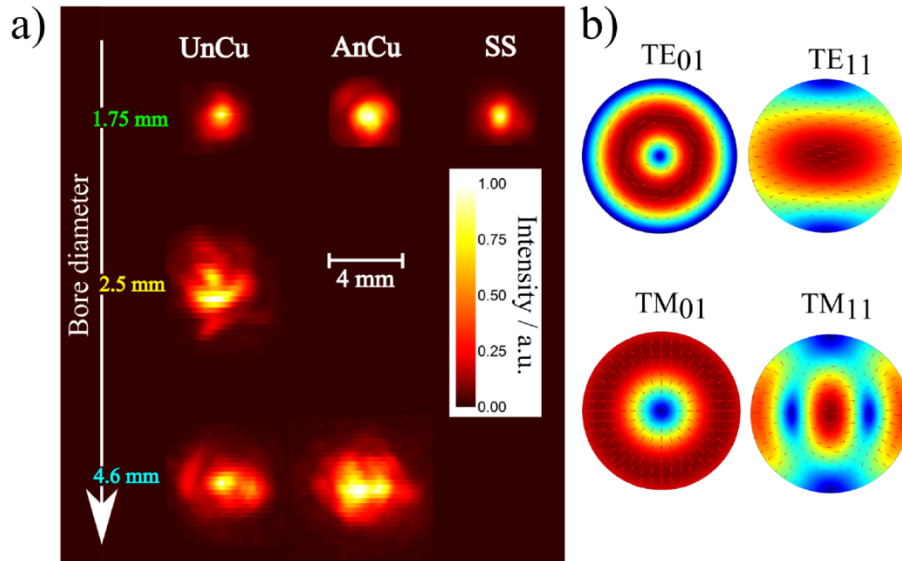


Fig. 5. a) Beam profiles of the HMWGs, measured at a distance of 4.5 mm using a Golay cell detector with 1 mm aperture. The top row shows profiles for 1.75 mm bore diameters (green), the middle 2.5 mm diameters (yellow) and the lower row 4.6 mm diameters (cyan). Primarily single mode transmission is observed for the 1.75 mm diameters. b) Theoretical lowest order modes supported in such cylindrical hollow metallic waveguides, as calculated by FEA simulations, showing the TE₀₁, TE₁₁, TM₀₁, and TM₁₁ modes.

Another important characteristic of any waveguide is the loss introduced upon bending the structure. This was measured by holding the input end of the HMWG aligned to the PS-MWG, and bending in the plane of polarization at a fixed bend radius for each diameter of waveguide. The power was measured from the end of the HMWG after each bend of 7.5° , up to a total of 90° . The bend radii used were 9.5, 12.7, and 15.9 mm, for the 1.75, 2.5, and 4.6 mm bore diameters respectively. Being purely metallic, when bent, the waveguides deformed in a ductile fashion into the desired bend, whilst retaining a constant inner diameter. The bend radii used here were chosen to represent realistic values for integration into cryogenic systems, as well as to be practical for optical benchtop measurements. The resulting losses introduced are shown in Fig. 6. The highest bending losses were observed for the 1.75 mm SS waveguide, showing a loss of ~ 7.5 dB at a bending angle of 90° . Conversely, the lowest bending losses of ~ 2 dB at 90° were observed for the 4.6 and 1.75 mm AnCu waveguides. Out of the range examined here, the combination of < 3 dB/m transmission losses, quasi-Gaussian beam profile and low bending losses, coupled with the high malleability and workability of the 4.6 mm AnCu waveguide, presents it as the most promising candidate for future cryogenic applications.

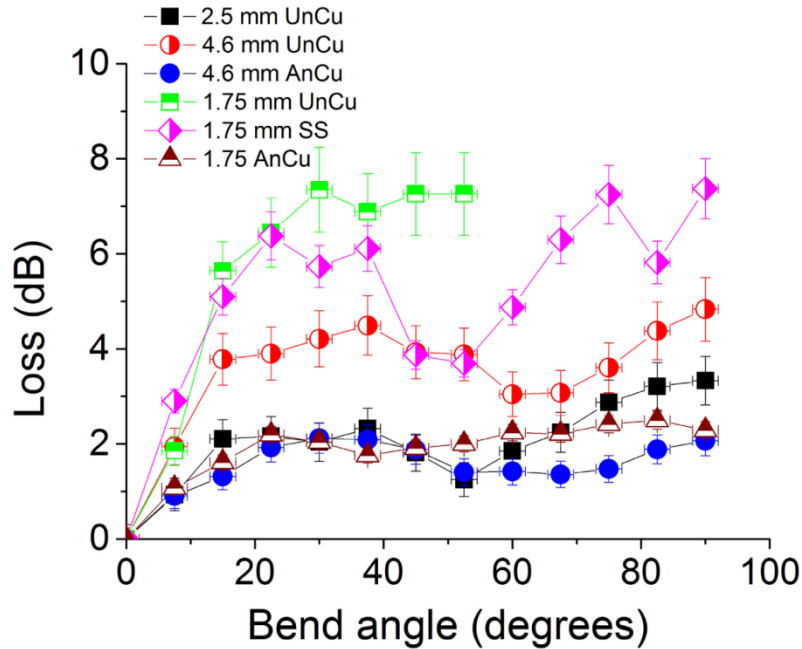


Fig. 6. Bending losses as a function of bend angle for a given diameter and material of waveguide. The bend radius for each diameter was fixed at a constant value - 9.5, 12.7, and 15.9 mm, for the 1.75, 2.5, and 4.6 mm diameters respectively. The lowest bend losses over the entire bend range were observed for the 4.6 mm AnCu waveguide.

4. Discussion

As was observed in Fig. 4, the transmission loss for a given waveguide tends to decrease with increasing bore diameter. A full idealized description of the variation in transmission losses, α_{lm} , of the lm^{th} mode, for a given wavelength and bore radius in such a waveguide, is given by [28]:

$$\alpha_{lm} = \left(\frac{u_{lm}}{2\pi} \right)^2 \frac{\lambda^2}{a^3} \text{Re}(v_l) \quad (1)$$

where u_{lm} is the mode parameter, equal to the zeros of the Bessel function, λ is the vacuum wavelength, a is the bore radius, and $\text{Re}(v_l)$ is a term which takes into account the mode supported, the geometry of the waveguide, and the complex refractive index of the metal in question. As can be seen from Eq. (1), the transmission losses are expected to scale with the inverse cube of the bore radius. Figure 7 plots the measured transmission loss for the UnCu waveguides against the three bore radii tested. As can be seen by fitting these data with an inverse cube relationship, for larger bore radii, there is a significant deviation from the idealized case described by Eq. (1). This deviation is suggested to be caused by two considerations. The first is that as the radius increases, a larger degree of higher order modes are introduced into the transmission, increasing the loss considerably, as can be seen in the u_{lm}^2 term of Eq. (1), and is consistent with previously reported hollow coated metallic waveguide structures [18].

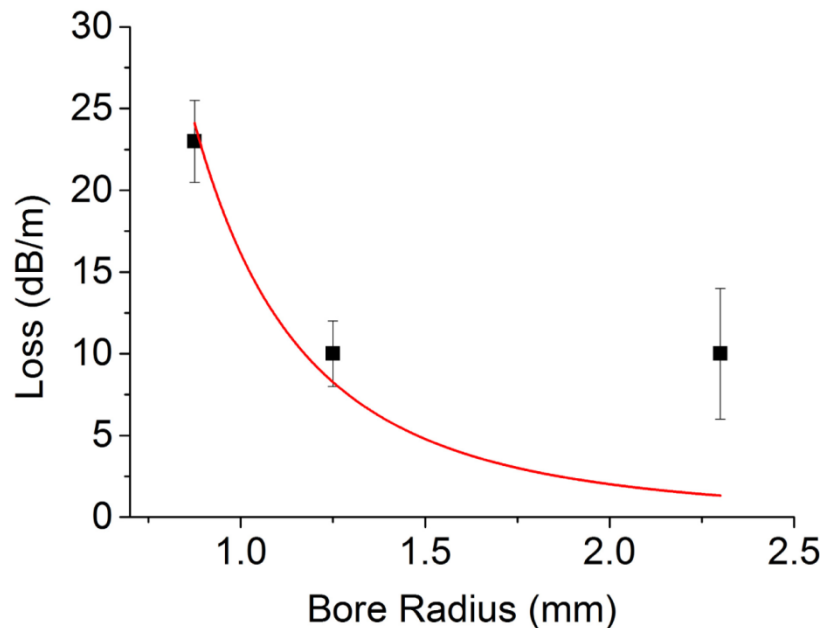


Fig. 7. Transmission loss as a function of bore radius for the three UnCu waveguides tested. The solid red line is an inverse cube fit, showing that the measured results deviate from the idealized case described in Eq. (1) for larger bore radii.

The second consideration is that Eq. (1) assumes perfectly smooth sidewalls, which is evidently an inaccurate assumption in the case of the waveguides investigated here, which have a degree of surface roughness on the inner bore. This surface roughness variation is also hypothesized to be a major contributing factor to another notable feature exhibited in Fig. 4, the reduction in transmission loss from UnCu to AnCu for a given frequency and diameter. In order to investigate the effect of the annealing process on the surface roughness parameters of the copper, and thus the interaction with the THz mode, a 5 mm length of 4.6 mm diameter UnCu and AnCu waveguide were cut down the axial direction to expose the inner surface. The roughness profile of the inner surfaces was measured using an AFM employing a probe tip with 50 nm radius of curvature, which was scanned in the axial direction of each waveguide over a distance of 2 mm, in 500 nm steps, whilst maintaining a height of approximately 50 nm above the sample surface. The resulting profiles are shown in Fig. 8 for UnCu (top left) and AnCu (bottom left). The two main parameters required for making a quantitative comparison of the two surfaces were then determined. These were the RMS surface roughness, σ , which measures the surface roughness in the vertical (z) direction, and the correlation length, L_c , which is obtained by the autocorrelation function of the acquired profile, and is related to the dispersive properties of the scattering losses. Values of σ for UnCu and AnCu were estimated from the data to be 2.9 and 1.6 μm respectively. The correlation length was estimated by fitting the magnitude of the power spectral density of the profiles with an exponential function $y = A \exp(-x/B)$, where A and B were free parameters and $L_c = 1/B$ [29], with values of $26 \pm 1 \mu\text{m}$ and $139 \pm 5 \mu\text{m}$ extracted for UnCu and AnCu respectively. From these extracted values, it is clear that there exists a significant difference in the properties of the inner surface between the annealed and un-annealed samples, with the AnCu surface varying on a considerably longer length scale.

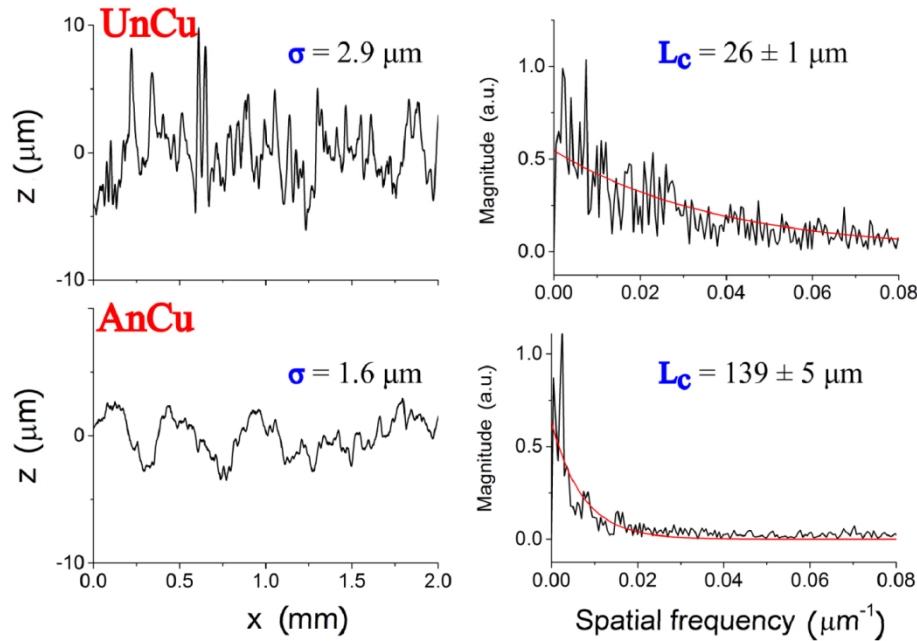


Fig. 8. Left panels - profiles of the inner surface of the 4.6 mm diameter UnCu and AnCu waveguides, recorded with a 500 nm step over a distance of 2 mm in the axial direction. Right panels - magnitude of the power spectral densities for each profile, with exponential fit (solid red line) to extract the associated correlation length. The correlation length of the AnCu varies on a significantly longer length scale.

In order to discriminate between the effect of the extracted σ and L_c values on the scattering loss component of the transmission losses, an experiment was conducted with the aim of retaining a constant correlation length, whilst varying the RMS roughness over the 1 – 3 μm range observed in the profiles in Fig. 8. This was achieved by preparing ten identical 100 mm long, 4.6 mm diameter AnCu waveguides. These were then cleaned as previously described, but with a modification to the nitric acid etching stage such that a pair of each of the set were exposed to a 1:2 $\text{HNO}_3:\text{H}_2\text{O}$ etching solution for one of the following times - 0, 10, 30, 60, and 120 seconds, with the aim of increasing the RMS roughness in proportion to the etch time, whilst leaving the correlation length unaltered. The surface parameters for each sample were then extracted in a similar manner as before using one of each of the pairs [Fig. 9(a)], whilst the unpurged transmission loss at 2.0 THz was measured for the other [Fig. 9(b)]. The extracted RMS roughness values show a generally increasing trend from $\sim 0.6 \mu\text{m}$ for the waveguide without a nitric etch, to 1.8 μm for 120 seconds etch time, whilst the correlation length remains constant at $\sim 100 \mu\text{m}$. However, the measured transmission loss was constant within the experimental uncertainty for all etch times, suggesting that the variation in RMS roughness between 2.9 and 1.6 μm for the UnCu and AnCu waveguides is not a contributing factor in the observed $> 6 \text{ dB/m}$ change in overall transmission loss measured in Fig. 4.

The dominant theoretical framework for these waveguides, which takes into account the RMS roughness, but not the correlation length, was developed for hollow cylindrical waveguides [30], and applied previously to silver coated waveguides [31]. The scattering losses, α , are related to the RMS surface roughness, σ , by

$$\alpha = -\left(\frac{4\pi\sigma \sin \theta}{\lambda}\right)^2 \quad (2)$$

where λ is the wavelength, and θ is the incident beam angle. For the measurements in Fig. 9, Eq. (2) suggests a scattering loss $\alpha < 0.1$ dB/m for a 2 THz beam for an RMS roughness value < 3 μm , confirming that the ratio between the RMS roughness and free space wavelength is too small to contribute significantly to the transmission losses in these experiments, and that this theory cannot fully describe the scattering losses in the waveguides investigated here.

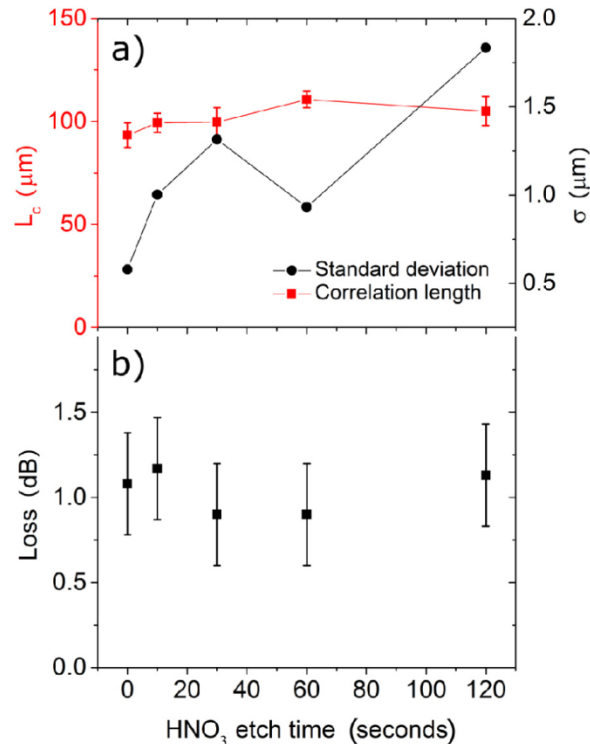


Fig. 9. a) Correlation length (red left axis) and RMS roughness (black right axis) as a function of HNO₃ etch time. The RMS roughness shows an increasing trend with etch time, whilst the correlation length remains comparatively constant. b) Measured transmission loss (unpurged) at 2.0 THz as a function of HNO₃ etch time, showing that the variation in RMS roughness on this scale has no influence on the transmission loss, within the experimental uncertainty.

In light of this, it is suggested that the change in transmission losses observed in Fig. 4 between the UnCu and AnCu waveguides is most likely due to the considerable variation in the correlation length of the respective inner surfaces, extracted in Fig. 8. The data may suggest that backscattering, arising from constructive interference due to the periodic surface corrugations, is responsible for the increased losses in some waveguides, however the current set of data cannot prove this conclusively. Another potentially appropriate description may be Mie scattering theory, which predicts oscillating values of the scattering cross section when the size of the scattering elements is comparable to the wavelength, but is not well suited here as such dimensions are not uniquely identifiable in this case. In the literature, Lee *et al.* [32] demonstrated that buried waveguides have shown peak scattering losses for values of the incident wavelength around $\lambda/4$, which is also suggested by our data. A set of waveguides spanning a wider range of RMS roughness values and correlation lengths, and also over several frequencies, is required in order to rule out precisely which, among all these effects, best describes the scattering losses in these waveguides. Additionally, a more comprehensive modelling of the interaction between the optical mode distributions and the measured waveguide surfaces would be insightful. However, the development of a scattering theory to

describe such effects in the waveguides presented here, although both interesting and useful, is beyond the scope of the present manuscript.

5. Conclusion

In this work, the transmission losses, mode profiles, and bending losses of cylindrical hollow copper and stainless steel waveguides with diameters between 1.75 and 4.6 mm have been investigated, with a view to meeting the requirements of future THz cryogenic applications. Transmission losses < 3 dB/m at 2.0 THz have been observed for a N_2 purged 4.6 mm bore diameter annealed Cu waveguide, as well as 90° bending losses as low as ~ 2 dB/m with a bend radius of 15.9 mm. Single mode transmission has also been demonstrated for a bore diameter of 1.75 mm. The influence on the recorded transmission losses of the inner waveguide surface RMS roughness and correlation lengths has also been explored, with the relative influence of parameters being effectively distinguished, and compared to the corresponding theoretical frameworks available. The results presented here pave the way for a new generation of cryogenic applications requiring efficient and targeted power delivery in the THz regime.

Funding

Engineering and Physical Sciences Research Council (Grant No. EP/J017671/1, Coherent Terahertz Systems).

Acknowledgments

Additional data sets related to this publication are available from the Cambridge University data repository at <http://dx.doi.org/10.17863/CAM.6166>.